J Biol Inorg Chem (2001) 6: 778–790
DOI 10.1007/s007750100254

ORIGINAL ARTICLE

S. Benini · W.R. Rypniewski · K.S. Wilson · S. Ciurli
S. Mangani

Structure-based rationalization of urease inhibition by phosphate: novel insights into the enzyme mechanism

Received: 2 February 2001 / Accepted: 30 April 2001 / Published online: 27 June 2001

Abstract The structure of *Bacillus pasteurii* urease (BPU) inhibited with phosphate was solved and refined using synchrotron X-ray diffraction data from a vitrified crystal (1.85 Å resolution, 99.3% completeness, data redundancy 4.6, *R*-factor 17.3%, PDB code 6UBP). A distance of 3.5 Å separates the two Ni ions in the active site. The binding mode of the inhibitor involves the formation of four coordination bonds with the two Ni ions: one phosphate oxygen atom symmetrically bridges the two metal ions (1.9–2.0 Å), while two of the remaining phosphate oxygen atoms bind to the Ni atoms at 2.4 Å. The fourth phosphate oxygen is directed into the active site channel. Analysis of the H-bonding network around the bound inhibitor indicates that phosphate is bound as the $H_2PO_4^-$ anion, and that an additional proton is present on the Oδ2 atom of Asp$^{\alpha 363}$, an active site residue involved in Ni coordination through Oδ1. The flexible flap flanking the active site cavity is in the open conformation. Analysis of the complex reveals why phosphate is a relatively weak inhibitor and why sulfate does not bind to the nickels in the active site. The implications of the results for the understanding of the urease catalytic mechanism are reviewed. A novel alternative for the proton donor is presented.

Keywords Urease · *Bacillus pasteurii* · X-ray diffraction · Nickel · Phosphate

Abbreviations *AHA*: acetohydroxamic acid · *BME*: β-mercaptoethanol · *BPU*: *Bacillus pasteurii* urease · *DAP*: diamidophosphate · *DFT*: density functional theory · *JBU*: jack bean urease · *KAU*: *Klebsiella aerogenes* urease · *NAT*: native enzyme · *PHO*: phosphate · *PPD*: phenyl phosphorodiamidate

S. Ciurli (✉)
Department of Agro-Environmental Science and Technology, University of Bologna, Viale Berti Pichat 10, 40127 Bologna, Italy
E-mail: sciurli@agrsci.unibo.it
Fax: +39-051-243362

S. Mangani
Department of Chemistry, University of Siena, Via Aldo Moro, 53100 Siena, Italy
e-mail: mangani@unisi.it
Fax: +39-0577-234233

S. Benini · W.R. Rypniewski
EMBL, c/o DESY, Notkestrasse 85, 22603 Hamburg, Germany

K.S. Wilson
Structural Biology Laboratory, Department of Chemistry, University of York, Heslington, York, YO10 5DD, UK

Present address: S. Benini
International Center for Genetic Engineering and Biotechnology, DNA Replication Group, Padriciano 99, 34012 Trieste, Italy

Introduction

Competitive phosphate inhibition of urease (urea amidohydrolase, E.C. 3.5.1.5), a nickel-containing metalloenzyme, was first described in 1934 [1] and later confirmed by several authors [2, 3, 4, 5, 6]. The elucidation of the urease-phosphate interaction at the molecular level should lead to a deeper understanding of the mechanism of catalysis. Two detailed investigations have been reported, dealing with the kinetic characterization of the interaction between phosphate and *Klebsiella aerogenes* urease (KAU) [5] and jack bean (*Canavalia ensiformis*) urease (JBU) [7]. JBU consists of six subunits, each made of 840 amino acids [8, 9], while KAU has an $(\alpha\beta\gamma)_3$ quaternary structure, with 101, 106, and 567 residues in the α, β, and γ subunits, respectively [10]. The $\alpha\beta\gamma$ fragment of KAU is highly homologous to the single subunit of JBU [11].

Phosphate competitively inhibits KAU in the pH range 5.0–7.0. The inhibition is weak and not purely competitive at pH > 7.0, while the enzyme is labile at

pH < 5.0. Within the pH range 5.0–7.0 the inhibition is pH dependent, with values of K_i increasing from ca. 0.1 mM at pH 5 to ca. 50 mM at pH 7. Within this pH range, pK_i exhibits a slope of –1 from pH 5.0 to 6.3, and a slope of –2 from pH 6.3 to 7.0. These results suggest that phosphate inhibition of urease requires protonation of two ionizable groups with pK_{a1} = 6.3 and pK_{a2} < 5 [5].

Similar results were more recently obtained for JBU [7], where the pH dependence of phosphate inhibition was investigated in the range 5.8–8.1. It was shown that phosphate is a competitive inhibitor in the pH range 5.8–7.5, with K_i values increasing from 0.53 mM at pH 5.8 to 123 mM at pH 7.5. Similar to KAU, the slope of pK_i versus pH was –1 in the pH range 5.8–6.5 and –2 in the range 6.5–7.5. These results revealed the existence of two ionizable groups having dissociation constants corresponding to pK_{a1} = 6.5 (similar to the value of 6.3 observed for KAU) and pK_{a3} = 7.2. At pH values higher than 7.6 there was no competitive inhibition. The interpretation of the kinetic data led the authors to suggest that pK_{a3} corresponds to the deprotonation of the true inhibitor, the $H_2PO_4^-$ anion [7].

Comprehensive analysis of these data, together with the established conservation of the active site residues in KAU and JBU [11], leads to the conclusion that phosphate inhibition of urease involves three protonation sites, with pK_a values of ca. 7.2, 6.5, and < 5. Several different inhibition mechanisms can therefore be proposed, depending on whether the three values of pK_a are associated with the inhibitor or with active site residues.

In the absence of structural details for a phosphate-urease complex, the following interpretation of the overall kinetic data were inferred [5, 7]. The enzyme active site was known to contain a group with pK_a = 6.5, assigned to a histidine residue [12, 13], suggesting the assignment of pK_{a1} to this residue. Moreover, the kinetic data on JBU strongly supported the view that the pK_{a3} of 7.2 corresponds to the deprotonation of the $H_2PO_4^-$ anion. This would leave the lowest pK_{a2} (< 5) assigned to either the first deprotonation of H_3PO_4 (pK_a = ca. 2) or to a deprotonation of an active site residue (possibly a carboxylate group of Asp or Glu).

The determination of the native (NAT) structures of two microbial ureases, from *K. aerogenes* [14] (PDB code 1FWJ, resolution 2.0 Å) and *Bacillus pasteurii* [15] (PDB code 2UBP, resolution 2.0 Å), provides a reliable background for a better understanding of the inhibition mechanism by phosphate. These two ureases are essentially identical in terms of backbone structure. In particular, the three α subunits, constituting the core of the $(\alpha\beta\gamma)_3$ trimer, consist of an $\alpha\beta$ barrel domain and a β-type domain. In turn, the β subunits, located on the surface of the trimer, feature a predominantly β structure. Finally, the γ subunits consist of $\alpha\beta$ domains located on top of each pair of α subunits, favoring their association to form the trimer of trimers. The structures also reveal a highly conserved position of the metal ions and the amino acid residues in the active site [16].

In the structure of native *B. pasteurii* urease (BPU), two Ni ions are bridged by the carboxylate group of the carbamylated $Lys^{\alpha 220*}$, bound to Ni(1) through Oθ1 and to Ni(2) through Oθ2. Ni(1) is further coordinated by $His^{\alpha 249}$ Nδ and $His^{\alpha 275}$ Nϵ, while Ni(2) is bound to $His^{\alpha 137}$ Nϵ, $His^{\alpha 139}$ Nϵ, and $Asp^{\alpha 363}$ Oδ1 (Fig. 1A). The Ni-Ni distance is 3.7 Å. The coordination geometry is pseudo square pyramidal for the penta-coordinated Ni(1) and pseudo octahedral for the hexa-coordinated Ni(2), in agreement with EXAFS data on native BPU [17]. Four water/hydroxide molecules constitute a tetrahedral cluster in the active site; one of these (W_B) symmetrically bridges the two Ni ions, and was proposed to be in the hydroxo form, while two additional water molecules, W_1 and W_2, bind Ni(1) and Ni(2), respectively. The fourth water (W_3) is not involved in any coordination bonds with Ni, but is H-bonded to the first three solvent molecules [15, 16].

The structures of BPU complexed with several inhibitors have also been determined. In BPU inhibited with β-mercaptoethanol (BME) (PDB code 1UBP, resolution 1.65 Å) the thiolate atom symmetrically bridges the binuclear Ni center, with a Ni-Ni distance of 3.1 Å. BME further chelates Ni(1) via its terminal OH [16, 18] (Fig. 1B), resulting in both Ni ions being penta-coordinate. The structure of BPU inhibited with acetohydroxamic acid (AHA) (PDB code 4UBP, resolution 1.55 Å) shows the inhibitor symmetrically bridging the two penta-coordinate Ni ions in the active site through the hydroxamate oxygen. The Ni ions are separated by 3.53 Å. The inhibitor further chelates one Ni ion through the carbonyl oxygen [19] (Fig. 1C). In crystals of BPU obtained from solutions containing phenyl phosphorodiamidate (PPD, PDB code 3UBP), a molecule of its enzymatic hydrolysis product, diamidophosphoric acid (DAP) [20], is coordinated to Ni(1) and to Ni(2) using three of the four atoms potentially available for coordination (Fig. 1D). One oxygen atom of DAP, originally identified as a P-OH group [15] and later proposed to be the anionic P-O^- moiety [21], bridges the two Ni ions, while one oxygen and one nitrogen atom bind to Ni(1) and Ni(2), respectively. The second nitrogen atom of DAP points away towards the cavity opening [15, 16]. The Ni-Ni distance is 3.8 Å. The binding of DAP does not change the coordination geometry of the Ni ions with respect to the native enzyme, consistent with EXAFS studies reported for PPD-inhibited BPU [17].

The present report describes the structure determination of BPU crystallized in the presence of phosphate (PHO). This is the first structure of a urease complexed with phosphate, and reveals the unexpected tridentate binding mode of this inhibitor. The structure of the PHO-BPU complex provides a rationale for the kinetic data on phosphate inhibition, and suggests a mechanism for the formation of the phosphate-urease complex, allowing some deeper insights into the enzymatic catalysis of urea hydrolysis.

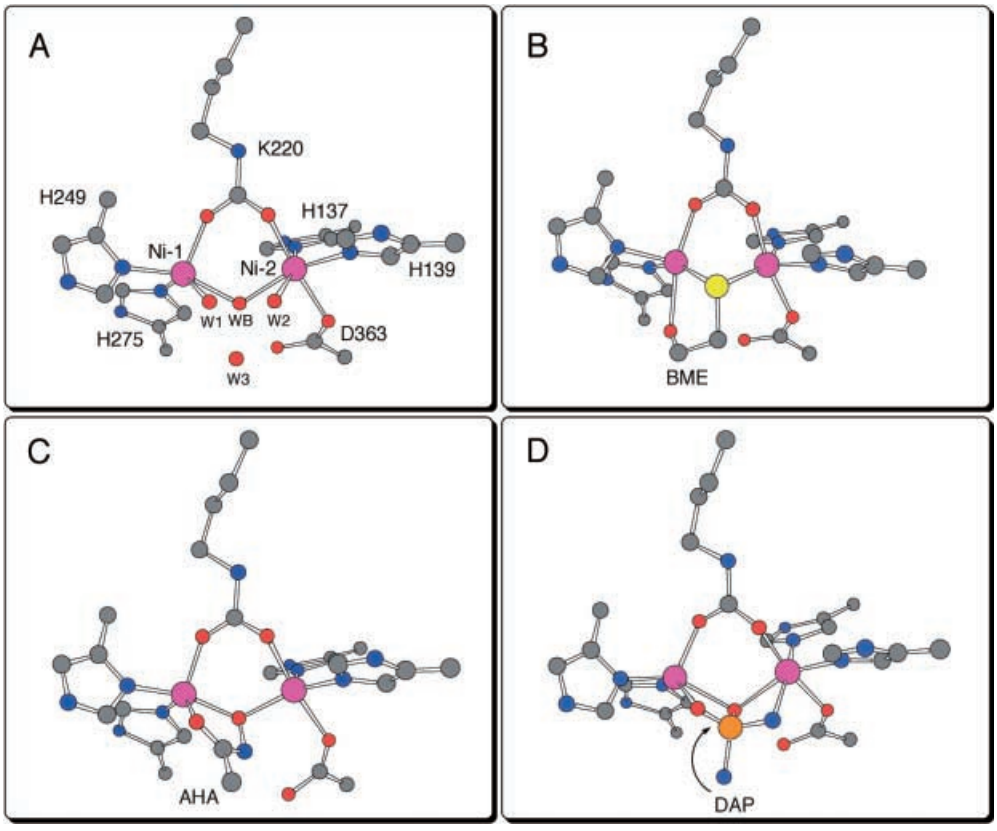

Fig. 1 Schemes for the active-site Ni coordination of native (**A**), BME-inhibited (**B**), AHA-inhibited (**C**), and DAP-inhibited (**D**) BPU. The CPK color scheme has been adopted for C, N, O, and S atoms. Ni and P are shown in *purple* and *orange*, respectively

Materials and methods

Protein isolation and crystallization

BPU was isolated and purified to a specific activity of ca. 2500 units/mg as previously reported [22]. Crystallization of phosphate-inhibited urease was achieved at 20 °C using the hanging drop method: 3 μL of a solution containing 11 mg/mL of urease in 50 mM sodium phosphate at pH 7.5, containing 50 mM Na_2SO_3, was diluted with 3 μL of the well solution (1.6–1.8 M ammonium sulfate in 100 mM sodium phosphate buffer, pH 6.3) and equilibrated against 500 μL of precipitant. The final pH was 6.8, measured on a larger volume prepared in a comparable manner. Rice-shaped single crystals, of about 0.4×0.4×0.7 mm^3 on average, formed in a few days.

Data collection and evaluation

Diffraction data were collected on a single crystal of the phosphate-inhibited BPU at 100 K using synchrotron radiation from the BW7B wiggler line of the DORIS storage ring at the EMBL outstation at DESY, Hamburg (Germany). The detector was a 30-cm MarResearch imaging plate scanner. For cryo-protection, a single crystal, of dimensions 0.3×0.3×0.5 mm^3, was transferred from the crystallization drop into 500 μL of the well solution, resulting in a final pH of 6.3. The concentration of the cryo-protectant was gradually increased from 0 to 15% by adding 100-μL portions of 20% ethylene glycol, at 1-min intervals. The crystal was transferred to a solution containing 20% ethylene glycol, scooped up in a cryo-loop and rapidly exposed to a cold nitrogen stream. The pH of the crystal after this treatment was not measured, but is assumed to be close to 6.3.

The data were processed using the program DENZO and merged with SCALEPACK [23] (Table 1). The high-resolution limit (1.85 Å) was chosen so that at least 50% of the reflections in the highest shell had $I/\sigma(I)$ of 1.85, just below the value of 2 recommended by Dauter [24]. The cell is isomorphous with that of the native enzyme (Table 1) and contains four urease molecules lying on the special positions of point symmetry three. Therefore the asymmetric unit consists of one third (one $\alpha\beta\gamma$ moiety [15]) of the $(\alpha\beta\gamma)_3$ urease molecule.

Table 1 X-ray data collection statistics and data reduction for phosphate-inhibited BPU

Wavelength (Å)	0.834
Resolution range (Å)	30.00–1.85
R_{merge}[a]	0.097
Raw measurements	381,291
Unique reflections	82,718
Redundancy	4.61
High resolution bin (Å)	1.88–1.85
% Completeness	99.3
% Completeness in high resolution bin	94.3
% Greater than 3σ	63.4
% Greater than 2σ in high-resolution bin	48.0
Redundancy in high-resolution bin	3.2
I/σ	10.2
I/σ in high-resolution bin	1.85
Space group	$P6_322$
$a=b$ (Å)	131.49
c (Å)	189.49

[a] $R_{merge}=\Sigma|I_i-<I>|/\Sigma<I>$, where I_i is an individual intensity measurement, and $<I>$ is the average intensity for this reflection with summation over all the data

Structure determination and refinement

Initial phases were obtained from the refined model of the native enzyme (PDB code 2UBP [15]) from which the sulfate anion, the

flexible loop region, and all water molecules were omitted. The protein regions displaying different conformations were manually rebuilt with the program O [25]. The structure was refined using REFMAC [26] with established geometric targets [27] (Table 2). Randomly selected reflections (2% of the total) were used as an R_{free} set for cross validation. Automatic solvent building was performed using the program ARP, keeping only those water molecules having density greater than 1.5σ in the $2F_o$–F_c electron density map [28]. No restraints were imposed on the Ni-ligand distances. The phosphate molecule was refined using an occupancy of 65%, estimated by keeping the ratio of the Ni/inhibitor *B*-factors similar to that observed for the DAP-urease complex [15]. Omit maps were calculated after several refinement cycles of a model from which the phosphate atoms were excluded. Using isotropic temperature factors the refinement converged to *R* and R_{free} of 17.3% and 21.1%, respectively. The stereochemistry of the final model was checked using the programs WHATIF [29] and PROCHECK [30]. The refined crystallographic coordinates and structure factor amplitudes for phosphate-inhibited BPU have been deposited in the Protein Data Bank under the accession code 1IE7.

Results and discussion

Overall structure of phosphate-inhibited BPU

The $(\alpha\beta\gamma)_3$ quaternary structure of the phosphate-inhibited BPU is unchanged from that observed in previous studies of the *B. pasteurii* and *K. aerogenes* microbial enzymes. The structure is very similar to that of native BPU with an overall RMSD of only 0.14 Å based on the superposition of the complete set of Cα atoms of the three subunits.

A comparison of ϕ and ψ backbone angles adopted by the polypeptide chain in the BPU structures determined to date reveals some interesting features. The values of $\Delta\phi$ and $\Delta\psi$ between the native enzyme and all inhibited forms for the β- and γ-subunits are small (RMSD within the 3.6–5.5° range), while the α-subunits show some important differences. Figure 2 shows the values of $\Delta\phi$ and $\Delta\psi$ between the α subunits of native and inhibited BPU. All structures differ significantly only in two regions, involving residues 366–367 (region A) and 395–397 (region B). The ϕ and ψ angles of region A undergo a shift of ca. 250° and 100°, respectively, for DAP- and PHO-inhibited BPU, while they are the same as in the native in the BME- and AHA-inhibitor complexes. The ϕ and ψ angles of region B, in contrast, undergo a shift of ca. 150–200° and 250°, respectively, for the BME-, DAP- and PHO-inhibited BPU, while in the AHA-inhibitor complex they are the same as in the native.

Table 2 Summary of the crystallographic analysis and refinement for phosphate-inhibited BPU

Protein atoms	6054
Solvent atoms	896
Bound metal ions	2 Ni
Bound inhibitor atoms	5
Temperature factors for protein atoms (Å^2)	28.5
Temperature factors for solvent (Å^2)	48.0
Temperature factors for Ni(1), Ni(2) (Å^2)	36.63, 34.90
Average temperature factors for PO_4 atoms (Å^2)	37.69
RMS bond length deviation (Å)	0.012
RMS bond angle deviation (°)	0.033
RMS planes deviation (°)	0.044
RMS on atomic positions from σ_A plots (Å)	0.067
RMS on final $2F_o$–F_c electron density map (electrons/Å^3)	0.26
Ramachandran most favored region (%)	89.6
Ramachandran additional allowed region (%)	9.2
Ramachandran generously allowed region (%)	1.1
R-factor (*R*-free)[a] (%)	17.3 (21.0)

[a] $R\text{-factor} = \Sigma||F_o|-|F_c||/\Sigma|F_o|$; *R*-factor and *R*-free are calculated by using the working and free reflection sets, respectively; the free reflections (2% of the total) were held aside throughout the refinement

Region A, located close to the Ni ions and comprising residues Ala$^{\alpha366}$ and Met$^{\alpha367}$ (highly conserved in all ureases [11]), adopts two main conformations. These are hereafter named α (with the carbonyl group of Ala$^{\alpha366}$ pointing *away* from the Ni ions, as found in NAT-BPU, BME-BPU, and AHA-BPU) and β (with the carbonyl group of Ala$^{\alpha366}$ pointing *towards* the Ni ions, as found in DAP-BPU and PHO-BPU) (Fig. 3A). Region B, including the non-conserved residues Lys$^{\alpha395}$-Asn$^{\alpha396}$-Gly$^{\alpha397}$, is more flexible and assumes a range of conformations spanning differing values of ϕ and ψ (Fig. 3B). This different type of flexibility for regions A and B is confirmed by the significantly larger *B*-factors for region B in all BPU structures determined to date [19], as well as in the present structure, while the *B*-factors for region A are invariantly small. Region B is part of a loop positioned on the exterior of the protein, 40 Å away from the active site, and is not involved in any inter-subunit interface; its conformational flexibility is assumed not to be relevant to catalysis.

Figure 2 shows an additional perturbation of the backbone dihedral angles in all complexes in the region comprising residues 310–340 of the α subunit. This region includes a helix-loop-helix motif known to be part of the flexible flap covering the active site cavity [15, 16, 18, 31]. This flap has been crystallographically observed in two main conformations, "closed" or "open", and has been proposed to modulate the catalytic activity of the enzyme [15, 16, 31, 32]. The residues in this region, for the PHO-inhibited structure, have significantly larger *B*-factors than in other regions of the protein, indicating disorder, and therefore conformational flexibility, of this motif in the crystal. This flexibility is common to all known structures of BPU [19]. In this region the residue-averaged *B*-factor for PHO-inhibited BPU reaches a maximum value of ca. 60 Å^2 in the loop connecting the two helices (residues 326–331), while the average value for the protein is ca. 37 Å^2. The electron density from $2F_o$–F_c maps at the 0.5σ level is however sufficiently clear to allow us to build a reliable structural model. Figure 3C reveals that the flexible flap predominantly adopts the "open" conformation. This conformation has also been observed in NAT-BPU [15] as well as in BME-BPU [18] and AHA-BPU [19], while the flap is "closed" in DAP-BPU [15] (Fig. 3C). It is interesting to notice that the flap is "closed" in native KAU [14].

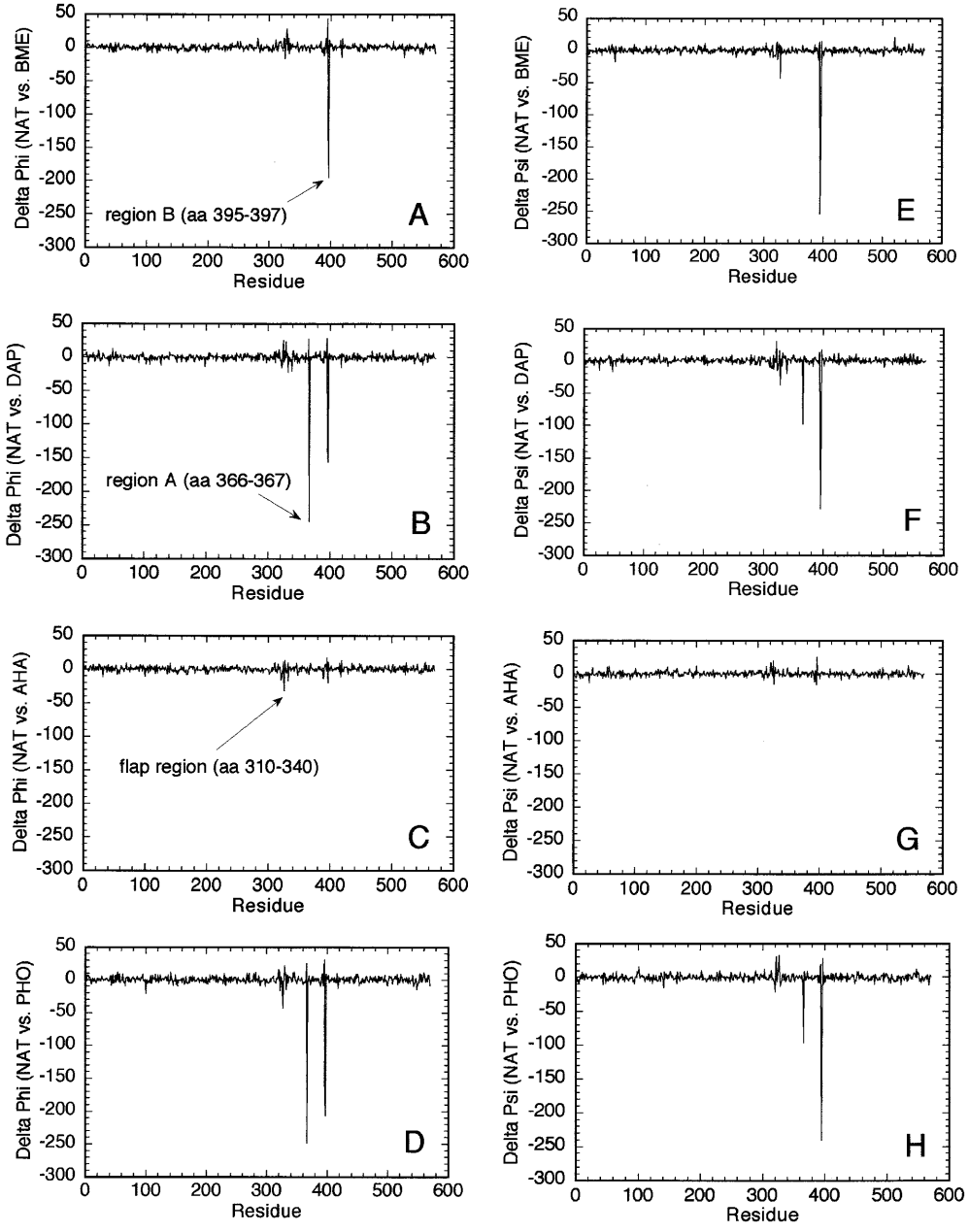

Fig. 2 Plots of $\Delta\phi$ (**A**, **B**, **C**, **D**) and $\Delta\psi$ (**E**, **F**, **G**, **H**) protein backbone angles between the native enzyme and BPU-BME (**A**, **E**), BPU-DAP (**B**, **F**), BPU-AHA (**C**, **G**), and BPU-PHO (**D**, **H**) inhibitor complexes for the *B. pasteurii* urease α-subunit. The amino acid residues defining region A, region B, and the flexible flap are indicated

It has been previously proposed that the conformations α and β of residues $Ala^{\alpha 366}$ and $Met^{\alpha 367}$ (region A) are correlated to the "open" and "closed" conformations of the flap, respectively [15]. The structure of PHO-inhibited BPU reported here, featuring a β conformation of region A and an "open" flap, clearly reveals that this correlation does not hold absolutely (see Fig. 3B, C). It is also evident from this analysis that region A is relatively free to adopt the α or β conformation, and that these two conformations constitute a sort of molecular switch between two thermodynamic minima, as revealed by the low *B*-factors always observed for this region regardless of the α or β conformation. This "dual flexibility" of region A may be important for the binding of both substrate and transition state during the catalytic mechanism, as discussed below.

The active site structure of phosphate-inhibited BPU and comparison with the native enzyme

The $2F_o$–F_c difference map (Fig. 4A) indicates that the arrangement of the protein ligands around the Ni ions in the PHO-BPU adduct is essentially identical to that observed in native BPU [15] (see Fig. 1A). The difference map shows a tetrahedral piece of electron density in the vicinity of the nickel ions, towards the open side of the active site channel. The density suggests the presence of a tetrahedral moiety bound to the binuclear nickel center through three atoms: one symmetrically bridges the two nickel atoms, with each of the other two atoms coordinated to one of the two nickels. The tetrahedral molecule has almost exactly replaced the cluster of four water/hydroxide molecules seen in native BPU, which was

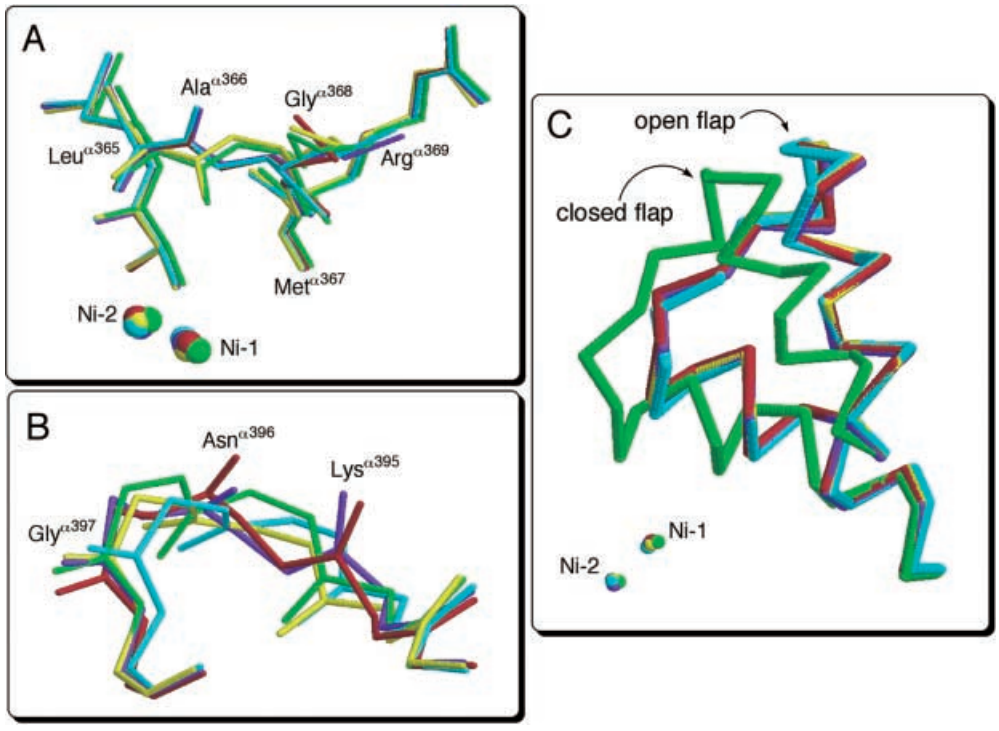

Fig. 3 Superposition of the protein atoms (**A**), backbone (**B**), and Cα (**C**) for region A (**A**), region B (**B**),and the active-site flap (**C**) of BPU structures colored according to the following scheme: native BPU = *red*; BPU-BME = *cyan*; BPU-DAP = *green*; BPU-AHA = *purple*; BPU-PHO = *yellow*

crystallized in the absence of phosphate [15]. Thus the presence of phosphate in the crystallization buffer in the present study has indeed allowed the binding of this weak inhibitor at pH 6.3, the assumed pH of the present crystal, even if not at full occupancy. This is in keeping with a pK_a of ca. 6.5 for the binding of phosphate to the active site of urease in BPU as measured for KAU [5] and JBU [7]. The final omit map, showing the inhibitor electron density, is shown in Fig. 4B.

The partial occupancy of 0.65 used for PHO in the refinement, and the weaker electron density observed for the "distal" phosphate oxygen with respect to the other inhibitor atoms, indicate that two different BPU structures are present in the crystal. Firstly, there is a low occupancy (~35%) native form (probably with even lower occupancy for the distal water molecule) and, secondly, a high occupancy (~65%) PHO-inhibited form. The diffraction data only permit an accuracy of 5–10% in the relative occupancies, but are of sufficient quality to reliably establish the presence of phosphate in roughly 65% of the urease molecules in the crystal.

The structure contains a single phosphate complexed to the Ni ions in the active site, with no other inhibitor molecule bound either in the cavity or to any other part of the protein. Figure 5 shows the model of phosphate bound to the bimetallic center, while Table 3 compares relevant distances in the active sites of the native and PHO-inhibited BPU structures. The Ni-bridging phosphate oxygen atom is symmetrically placed between the two metal ions (at 1.9 and 2.0 Å to Ni(1) and Ni(2), respectively). The O_B atom of phosphate replaces the bridging hydroxide molecule (W_B) present in native BPU [15], and causes shortening of the Ni(1)-Ni(2) distance by about 0.2 Å with respect to the native enzyme (see Table 3). This effect, although significant, is far less pronounced than that in BME-inhibited BPU, for which a decrease of 0.6 Å resulted from Ni-bridging by the thiolate atom of the inhibitor [18]. Two of the other phosphate oxygen atoms coordinate Ni(1) and Ni(2) at ligand distances of 2.4 Å, while the fourth ("distal") phosphate oxygen points towards the cavity opening, away from the two nickel ions. Thus, the four oxygen atoms of the bound phosphate closely mimic the cluster of four water/hydroxide molecules seen in native BPU. In all previous cases where a phosphate has been found bound to a binuclear metal site, it simply bridges the two metal ions in a chelate mode, leaving the bridging hydroxide in place [33]. Even in the inorganic models literature [34] there appears to be no case in which phosphate binds in the same mode as seen in BPU. The same is true for the unique case of DAP bound to BPU, i.e. with one atom (oxygen) of the tetrahedral inhibitor replacing the bridging hydroxide [15].

Nickel coordination in the phosphate complex

As a result of phosphate binding, Ni(1) is penta-coordinate, while Ni(2) is hexa-coordinate. The structural index parameter τ, introduced by Addison et al. [35], can be used to define better the geometry around the five-coordinate Ni(1) ion:

$$\tau = \frac{(\beta - \alpha)}{60} \quad (1)$$

According to this criterion, α and β ($\beta \geq \alpha$) are the two largest angles between any two coordinating atoms and the central atom, so that $\tau = 1$ for perfectly trigonal

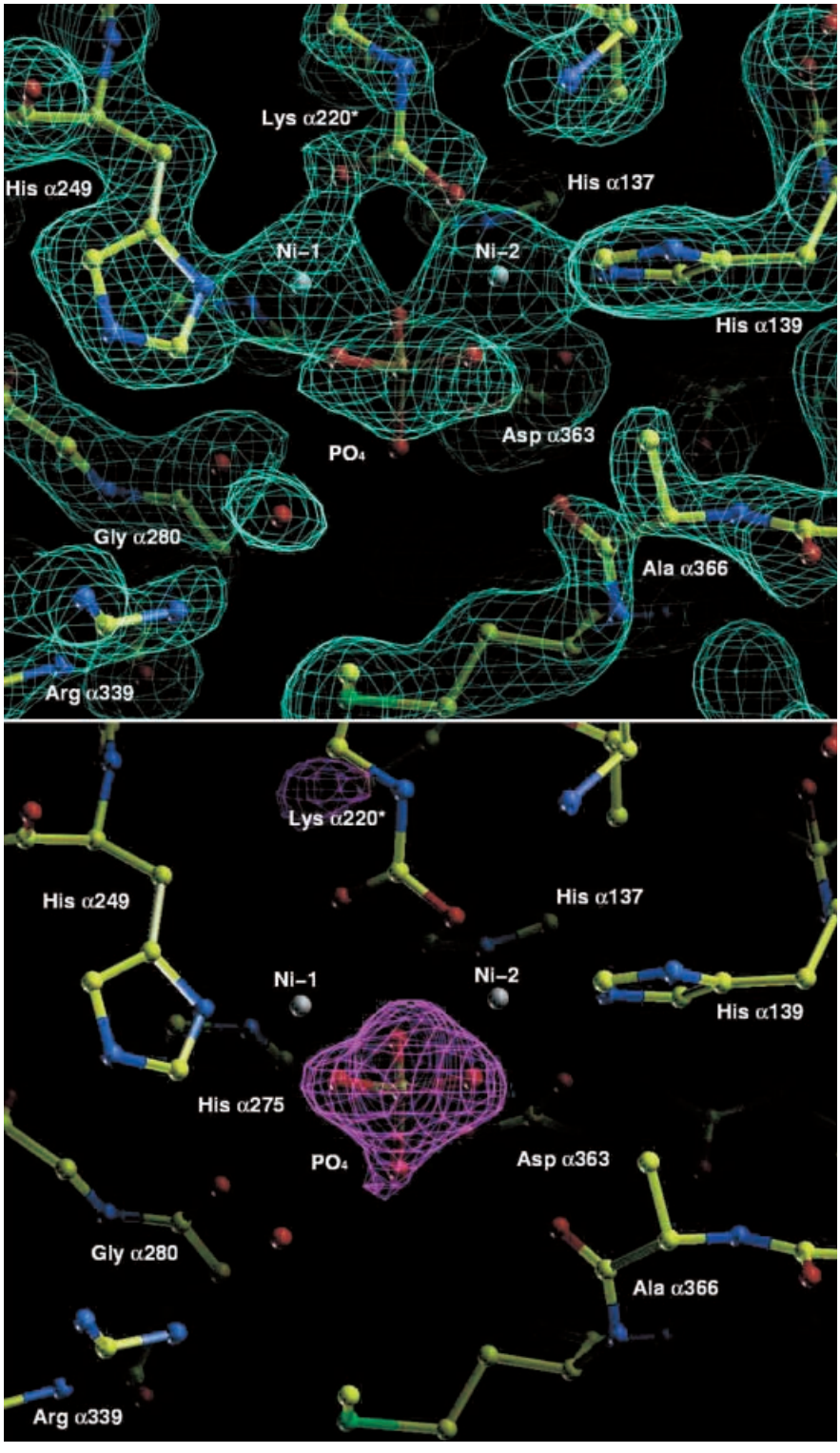

Fig. 4 **A** atomic model of the active site of PHO-inhibited BPU, showing the Ni coordination environment, superimposed on the final $2F_o–F_c$ electron density map contoured at 1.0σ. **B** omit map of the PHO molecule calculated with Fourier coefficients $F_o–F_c$ and phases derived from the final model from which the PHO atoms had been removed (*purple map*, contoured at 4.0σ)

bipyramidal (TB) geometry, whereas $\tau = 0$ for square-pyramidal (SPY) geometry. For five-coordinate structures the index τ can be used to describe the structural continuum between ideal SPY and TB geometry.

For phosphate-inhibited BPU, Scheme 1 holds for Ni(1).The value of $\tau = 0.283$ for Ni(1) can be compared with those obtained from the structures of DAP-inhibited BPU ($\tau = 0.067$, more SPY), native BPU ($\tau = 0.157$), BME-inhibited BPU ($\tau = 0.223$), and AHA-inhibited BPU ($\tau = 0.363$, more TB). These values indicate that Ni(1) has a preference for five-coordinate SPY geometry with various degrees of distortion toward a TB arrangement, as well as a significant flexibility of the coordination sphere.

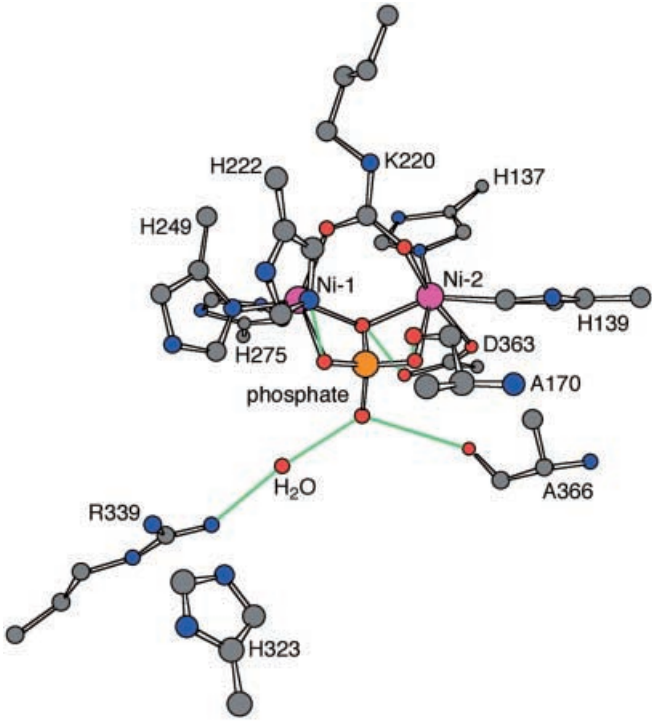

Fig. 5 Refined model of the active-site structure of PHO-inhibited BPU. The color scheme is the same as for Fig. 1. The *green lines* indicate significant H-bonds

Interaction of phosphate with the active site residues

The H-bonding network between the inhibitor atoms and the active site residues provides a clear definition of the protonation state of the bound phosphate (Fig. 5), as described by the following interactions:

1. The Ni(1)-bound phosphate oxygen atom must be deprotonated, as it receives a strong H-bond from the protonated $His^{\alpha 222}$ Nϵ (at 2.6 Å). As in all urease structures to date, the protonation state of the latter is dictated by the interaction of $His^{\alpha 222}$ Nδ with the peptide NH group of $Asp^{\alpha 224}$.
2. The Ni(2)-bound phosphate oxygen atom must be protonated, as it donates a strong H-bond to the carbonyl oxygen atom of $Ala^{\alpha 170}$ (at 2.8 Å).
3. The distal phosphate oxygen must be protonated, as it is within H-bonding distance (3.0 Å) of the carbonyl oxygen of $Ala^{\alpha 366}$ (in the β-conformation of region A, see above). This distal phosphate oxygen also receives an H-bond from a water molecule (at 2.8 Å), which additionally interacts with $Arg^{\alpha 339}$ through a strong charge-assisted H-bond.
4. The bridging phosphate oxygen is at H-bonding distance (2.8 Å) from $Asp^{\alpha 363}$ Oδ2, which in turn is at H-bonding distance (3.0 Å) from the "distal" phosphate oxygen. Only the former interaction, but not the latter, can involve a shared proton with $Asp^{\alpha 363}$ Oδ2, because the distal phosphate oxygen atom already bears a proton interacting with the carbonyl oxygen of $Ala^{\alpha 366}$. Thus the Ni-bound phosphate moiety is itself doubly protonated and a third hydrogen atom is shared between phosphate and $Asp^{\alpha 363}$ Oδ2 (Fig. 5).

Table 3 Selected distances and angles around the Ni centers in native, DAP-BPU, and PHO-BPU

	NAT-BPU	DAP-BPU	PHO-BPU
Ni-L distances (Å)			
Ni(1)-$Lys^{\alpha 220*}$ Oθ1[a]	2.1	2.1	2.1
Ni(1)-O_B[a]	2.1	2.3	1.9
Ni(1)-O_T[b]	2.2	2.2	2.4
Ni(1)-$His^{\alpha 249}$ Nδ	2.2	2.0	2.0
Ni(1)-$His^{\alpha 275}$ Nϵ	2.2	2.1	2.0
Ni(2)-$Lys^{\alpha 220*}$ Oθ2	2.1	1.9	2.0
Ni(2)-O_B	2.2	2.3	2.0
Ni(2)-O_T (N_T)	2.1	2.3	2.4
Ni(2)-$His^{\alpha 137}$ Nϵ	2.2	2.1	2.1
Ni(2)-$His^{\alpha 139}$ Nϵ	2.2	2.2	2.2
Ni(2)-$Asp^{\alpha 363}$ Oδ1	2.2	2.1	2.2
Ni(1)···Ni(2)	3.7	3.8	3.5
L-Ni-L angles (°)			
$Lys^{\alpha 220*}$ Oθ1-Ni(1)-$His^{\alpha 249}$ Nδ	105	111	110
$Lys^{\alpha 220*}$ Oθ1-Ni(1)-$His^{\alpha 275}$ Nϵ	111	106	110
$Lys^{\alpha 220*}$ Oθ1-Ni(1)-O_T	104	103	116
$Lys^{\alpha 220*}$ Oθ1-Ni(1)-O_B	95	95	92
$His^{\alpha 249}$ Nδ-Ni(1)-$His^{\alpha 275}$ Nϵ	95	103	92
O_T-Ni(1)-O_B	58	67	71
O_T-Ni(1)-$His^{\alpha 275}$ Nϵ	140	143	133
$His^{\alpha 249}$ Nδ-Ni(1)-O_B	149	147	150
$Lys^{\alpha 220*}$ Oθ2-Ni(2)-$His^{\alpha 137}$ Nϵ	94	90	97
$Lys^{\alpha 220*}$ Oθ2-Ni(2)-$His^{\alpha 139}$ Nϵ	88	94	96
$Lys^{\alpha 220*}$ Oθ2-Ni(2)-O_T (N_T)	91	99	89
$Lys^{\alpha 220*}$ Oθ2-Ni(2)-O_B	98	100	92
$His^{\alpha 137}$ Nϵ-Ni(2)-$His^{\alpha 139}$ Nϵ	113	108	117
O_B-Ni(2)-O_T (N_T)	63	71	69
$Lys^{\alpha 220*}$ Oθ2-Ni(2)-$Asp^{\alpha 363}$ Oδ1	175	168	171
$His^{\alpha 137}$ Nϵ-Ni(2)-O_T (N_T)	157	162	160
$His^{\alpha 139}$ Nϵ-Ni(2)-O_B	152	155	150
Ni(1)-O_B-Ni(2)	119	110	136

[a]The subscript B indicates the bridging atom
[b]The subscript T indicates the terminal atom

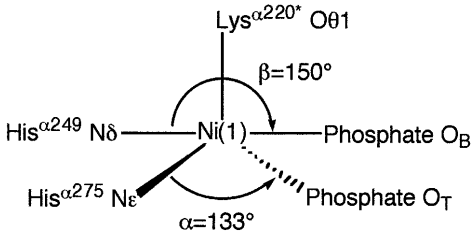

Scheme 1

The protonation state of the ligand allows a rationalization of the kinetic data on urease inhibition by phosphate [5, 7] as follows:

1. Urease is inactive below pH 5 but this probably reflects Ni ion loss and/or unfolding processes rather than protonation events in the active site. The first deprotonation of the H_3PO_4 to $H_2PO_4^-$ is likely to occur around pH 2, and is not relevant to the pH range discussed.

2. The PHO-BPU complex structure at the assumed pH of 6.3 shows that there are three protons directly involved in the interaction of phosphate with the urease active site, two on the phosphate and one shared between the phosphate bridging oxygen and $Asp^{\alpha 363}$ Oδ2. The order of acidity, or release, of these protons can be proposed to be:

(a) The most acidic proton is likely to be that shared between phosphate and $Asp^{\alpha 363}$ Oδ2. Loss of this proton probably corresponds to the ionization observed at pH 6.3–6.5 in the kinetic behavior of KAU and JBU. We propose the equivalent pK_a in BPU to be just above 6.3, perhaps influenced by the crystallization buffer and the crystal lattice, thereby justifying the estimated 65% occupancy of the active site by phosphate.

(b) Loss of the proton shared between the Ni(2)-bound phosphate oxygen and $Ala^{\alpha 170}$ corresponds to the ionization around pH 7.2 (and is formally related to the deprotonation of $H_2PO_4^-$ to yield HPO_4^{2-}).

(c) Release of the proton shared between the distal phosphate oxygen and $Ala^{\alpha 366}$ would leave a fully deprotonated phosphate moiety, and this step will only occur at pH considerably higher than 8.

An important conclusion from the present structure of PHO-inhibited BPU is that it provides an explanation for the relatively weak inhibition of the enzyme by phosphate. In particular, the increase in K_i over the pH range 5.0–7.0 can be ascribed to the increasing level of deprotonation of $H_2PO_4^-$ to HPO_4^{2-}, as this latter species lacks one of the two protons required to satisfy H-bonding to the two alanine carbonyl oxygen atoms. Above ca. pH 7.0, phosphate ceases to be an effective inhibitor.

In addition, the PHO-BPU model explains the strong discrimination between phosphate and sulfate. Sulfuric is a substantially stronger acid than is phosphoric, and the sulfate ion will be doubly charged throughout the active pH range of urease. This lack of protons to satisfy the carbonyl oxygen atoms of $Ala^{\alpha 170}$ and $Ala^{\alpha 366}$ clearly prevents its binding to the active site. This is in keeping with the native structure, where in spite of there being ca. 1 M ammonium sulfate in the crystallization buffer, there is no sulfate bound to the nickel ions in the active site [15]. Instead, a sulfate molecule is positioned roughly in the same position as the phosphate H-bonded water molecule in the PHO-BPU complex, interacting with $Arg^{\alpha 339}$ through a charge-assisted H-bond [15]. Very elegant examples of selective binding of phosphate and sulfate anions obtained by changing H-bond acceptors with H-bond donors in the anion binding cavity are provided by the crystal structures of the phosphate [36] and sulfate [37] binding proteins. The anion binding sites in the two proteins are very similar and the recognition between the protonated and the deprotonated anion is achieved by the presence of an aspartate group in the phosphate-binding site.

The mechanism reconsidered

It now seems appropriate to revisit the mechanism of catalysis in the light of the structures of both DAP-BPU and PHO-BPU complexes. It is generally accepted that, in the transition state, the urea molecule has been converted to a tetrahedral ion, having an sp^3 carbon and both N atoms also featuring sp^3 configuration. Starting from the ground state of urea, this involves three changes as discussed in the following subsections. The order of these changes is not clear and they could as well be viewed as a set of almost simultaneous events.

Mechanism step I: binding of urea in the active site

Model calculations [21] suggests that urea must first bind to the enzyme active site with the flap in the open conformation (this is supported by obvious steric clashes in the DAP and PHO complex structures for potential access of the ligand to the active site), with the urea O ligating Ni(1). Three of the four water molecules observed in the native structure are displaced, leaving only the bridging hydroxide. The structure of DAP-inhibited urease originally prompted us to propose that urea would also bind to Ni(2) through an NH_2 group [15, 16]. However, subsequent calculations [21] suggested that the formation of this bond is induced by flap closure, which decreases the active site volume available for the substrate molecule. Closure of the flap would also be responsible for the stabilization of the catalytic transition state through the formation of multiple H-bonds with active site residues (see below). The binding of the urea N to Ni(2) would be favored by the change of this N atom from "pseudo" sp^2 (with some sp^3 character, as established by DFT calculations [21]) to pure sp^3. The consequent loss of resonance delocalization energy of urea would be compensated by the formation of the urea N-Ni(2) coordination bond. The hybridization change of the urea N (and possibly the formation of the urea N-Ni(2) bond) should directly follow, or be concomitant with, the nucleophilic attack on the urea C by an incoming hydroxide. It is also possible that the partial sp^3 character of the N in unliganded urea is enough to induce the coordination bond with Ni(2), thereby favoring nucleophilic attack on the urea C by loss of resonance energy and decrease of electron density on the C atom itself.

Mechanism step II: nucleophilic attack by the bridging hydroxide to give the tetrahedral transition state

The structure of DAP-inhibited urease prompted us to propose a novel mechanism, which involved the Ni-bridging hydroxide as the nucleophile acting on the Ni-bound urea molecule [15]. This scheme was able to resolve several biochemical incongruities of the previously accepted mechanistic proposal, which involved as

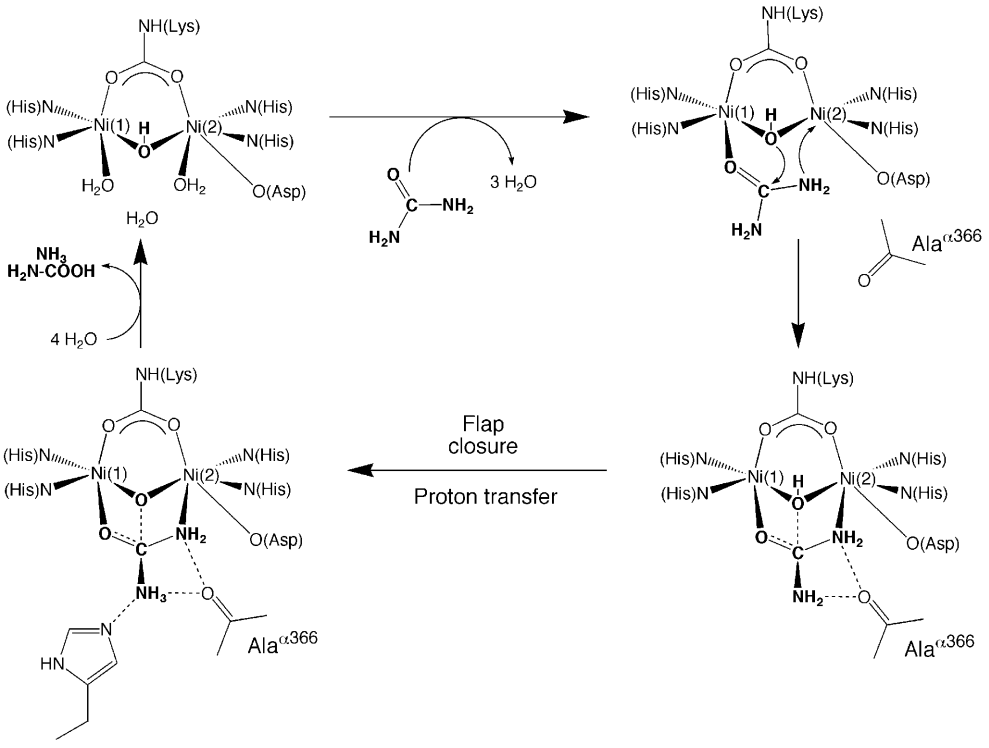

Fig. 6 Proposed mechanism for enzymatic catalysis by urease

the putative initial step the action of a Ni(2)-bound terminal hydroxide reacting with a substrate molecule bound to Ni(1) through the carbonyl oxygen [14, 31]. As stated above, it is not clear, and cannot easily be proven, whether the nucleophilic attack occurs after the formation of the urea N-Ni(2) bond (as suggested originally [15]) or concomitantly with it (as suggested later [21]).

Our "bridging hydroxide" mechanism initially raised some criticism based mainly on the supposed kinetic inertia of a doubly coordinated nucleophile[1]. A weakening of the Ni(1)-OH_B bond upon substrate binding could actually decrease such inertia. In fact, subsequent kinetic data on the inhibition of KAU with fluoride [38] and on KAU mutants [39], the structure and reactivity of inorganic models [40], and theoretical studies [21] support this proposal, which now seems to be generally accepted. The latter calculations also suggest the presence of a stable intermediate formed after the nucleophilic attack [21]. This result is consistent with the DAP complex being an excellent transition state analogue [15].

The nucleophilic attack by the Ni-bridging hydroxide onto the sp^2 carbon atom of the substrate yields a tetrahedral transition state containing an sp^3 carbon (Fig. 6). In the structures of BPU determined to date, two complexes represent direct analogues of this transition state: the present PHO-BPU complex and DAP-BPU [15]. In both structures the four oxygen or nitrogen atoms of the inhibitor lie in positions close to those of the four tetrahedrally arranged water molecules in the native enzyme, seen firstly and most clearly in the BPU model [15]. The two other complexes we have studied, BME [18] and AHA [19], have some atoms in equivalent positions to some of the waters, but show less overall similarity to the transition state and are not further discussed.

Comparison of the DAP- and PHO-BPU structures also reveals why phosphate [5, 7] binds much less strongly than DAP [20]. In the DAP complex the Ni(2)-bound DAP N atom donates two H-bonds to the carbonyl oxygen atoms of Ala$^{\alpha170}$ and Ala$^{\alpha366}$, while the distal DAP N atom is involved in H-bonding interactions with Ala$^{\alpha366}$ O, Gly$^{\alpha280}$ O, and His$^{\alpha323}$ Nϵ [15]. The corresponding distal and Ni(2)-bound protonated phosphate oxygen atoms in the PHO-BPU complex can each only donate a single hydrogen, and the binding is hence weakened by an energy roughly equivalent to two or three H-bonds.

Indeed, this optimization of H-bond donation from transition state to enzyme confers the exquisite specificity on urease: the substrate must be correctly oriented in the active site to achieve the appropriate H-bonding network, with sulfate or phosphate analogues expected, and found, to bind much more weakly. The structure of the real tetrahedral transition state will differ only slightly from that of the DAP structure, as the small volume of the carbon atom, as opposed to the phosphorus atom, will require its four ligands to contract and to form a somewhat smaller tetrahedron. As the positions of the Ni-bound and Ni-bridging ligand atoms are roughly fixed, the major effect is likely to be the move-

[1]This criticism was expressed during the XXXIII ICCC in Florence (August 1998), the 5th ISABC in Corfu (April 1999), and the 9th ICBIC in Minneapolis (August 1999)

ment of the carbon and distal oxygen atoms towards the two nickels compared to their positions in the PHO complex, and most likely closer to those seen for the waters in the native structure.

The structure of PHO-inhibited BPU further strengthens the view that the bridging hydroxide in urease is quite labile, as observed in all BPU complexes crystallographically determined so far [15, 16, 18, 19] and in inorganic models [40]. Concomitantly, the bridging hydroxide might be considered highly reactive, as indicated by the ability of the enzyme to hydrolyze PPD [20] and perhaps, we suggest, phosphate, where the enzyme would simply induce an oxygen atom (or hydroxide) exchange on the phosphate moiety. In this hypothetical framework, only molecules able to react with the bridging hydroxide may bind the enzyme in a tridentate mode, as observed for DAP and PHO. This would explain why DAP strongly inhibits urease when DAP itself is formed by enzymatic hydrolysis of phenyl phosphorodiamidate [PPD, C_6H_5-O-P(O)$(NH_2)_2$], whereas it is a weak inhibitor if externally added to the native enzyme [20].

Mechanism step III: protonation of the distal urea nitrogen followed by release of the first ammonium ion

It seems unlikely that the protonation of the urea NH_2 group is the initial driving force for the formation of the first tetrahedral transition state obtained upon nucleophilic attack of the bridging hydroxide, as the basic character of the urea N is very low. This is rather different from the situation observed, for example, in glycoside hydrolysis, where protonation of the glycosidic O by the COOH donor is one of the driving forces for the first step of the reaction (for a review see [41]). However, protonation of the distal N in the tetrahedral transition state is certainly the driving force for the C-N bond breakage. In turn, the driving force for this protonation would be the pK_a increase of the distal N upon, or after, nucleophilic attack. Consistent with these observations, DFT calculations have established that, upon nucleophilic attack of the bridging hydroxide on the urea C atom, the urea N atoms become sp^3 and their negative charge density increases, favoring protonation [21]. The same calculations also established that protonation of the intermediate formed upon nucleophilic attack by the hydroxide on the substrate urea does not yield another intermediate, but causes the breakage of the C-NH_3^+ bond and release of ammonia [21]. Therefore, only a second transition state must be attained before the enzymatic hydrolysis is completed. We have previously proposed that the stabilization of this transition state is attained, in urease, through the interaction of the nascent C-NH_3^+ group with $His^{\alpha323}$ Nϵ [15]. In this way, $His^{\alpha323}$ Nϵ would act as a base, stabilizing the proton on the distal urea N. The 10^3 reduction in k_{cat} on mutation of $His^{\alpha320}$ in KAU (corresponding to $His^{\alpha323}$ in BPU) [39] is understandable in this context. The structure of the PHO-BPU complex also reveals that another active site residue, $Ala^{\alpha366}$, could be important in regulating the protonation state of the distal NH_2 group. This residue can adopt two different conformations, α and β (see above), both thermodynamically stable, constituting a sort of ''molecular switch'' able to provide stabilization for the protonation of the distal urea NH_2 group.

A remaining point of contention in the mechanism is the source of the proton that gives rise to the distal C-NH_3^+ group. We currently see the three possibilities discussed below.

$His^{\alpha323}$ Nϵ as proton donor

Hausinger and co-workers [39], on the basis of kinetic studies on KAU mutants, have recently reiterated their original proposal involving $His^{\alpha323}$ as the proton donor to the urea NH_2 group. This proposal requires a so-called ''reverse protonation hypothesis'' [31] in order to circumvent the problem of having a residue ($His^{\alpha323}$) reported to have a p$K_a = 6.5$ in KAU [12, 13]) in a protonated state at the optimum pH for enzyme activity (ca. 8) in order to deliver the proton to a urea NH_2 group and form ammonia. The result of such reverse protonation is that only about 0.3% of the enzyme molecules are active at pH 8. On evolutionary grounds alone, it is very hard to accept this reverse protonation proposal: urea is a 250 kDa enzyme which has evolved to hydrolyze urea very fast and efficiently. Surely nature would have managed to select a proton donor which was fully protonated at the pH of optimal activity. Alternatively, it is possible that the pK_a value of 6.5 for $His^{\alpha323}$ relates to the open flap conformation, and that the pK_a increases upon flap closure [32].

In this respect, the major relevance of the PHO-BPU complex to an understanding of the mechanism is that $His^{\alpha323}$ must be deprotonated at the crystallization pH of 6.3. In fact, the structural data for the PHO-BPU complex clearly reveal that the active site flap is open, and that the side chain of $His^{\alpha323}$ (even though not modeled because of disorder) must be located far from the active site, not able to interact with the phosphate moiety. If this residue were protonated at this pH, it could further stabilize the inhibitor binding through the formation of an additional H-bond with the distal phosphate oxygen. The fact that such stabilization does not occur is an indication that the pK_a of $His^{\alpha323}$ may indeed be low, rendering it less likely to act as a proton donor during catalysis. In contrast, in DAP-inhibited BPU, $His^{\alpha323}$ Nϵ is involved in an H-bond with the distal N atom of the Ni-bound DAP [15]. This interaction does not require the protonation of $His^{\alpha323}$ Nϵ, which could act as an H-bond acceptor from the distal NH_2 group of DAP [15]. In the structure of DAP-inhibited BPU the active site flap is in the ''closed'' conformation, allowing $His^{\alpha323}$ to approach the Ni environment in the active site. In this view, the combined action of flap closure and $His^{\alpha323}$ H-bonding acceptor capability appears to play a role of a perfectly tuned device able to select the access

and stabilize the binding of molecules featuring, at the "distal" position, at least two or better three hydrogen atoms, as in DAP and urea. This analysis shows a particular advantage of BPU as opposed to KAU as a model, namely that the flap takes up one of two clear forms in the BPU crystals: open or closed. The open form is a necessity for initial urea binding; the closed form helps stabilize the transition state. In the native KAU structure, the only one available that does not involve mutations on the active site residues, the flap was found in the closed conformation [14]. Such difference, observed for the two enzymes in the native state, may be due to different crystal lattice forces favoring the closed over the open conformation for KAU, while leaving the flap in the BPU structures more free to adopt the most stable conformation, depending on the ligand present in the active site. In BPU, the flap only takes up the closed form, seemingly necessary for catalysis, in the DAP complex, containing the best transition state analogue. The free energy difference between the open and closed forms must be necessarily small to ensure that the change is reversible.

$Asp^{\alpha363}$ Oδ2 as proton donor

We had previously proposed, on the basis of the structure of the DAP-BPU complex, that the proton needed for protonation of the urea NH_2 group comes from the bridging hydroxide itself, through the $Asp^{\alpha363}$ Oδ2 atom, and that the proton is released from OH_B after the nucleophilic attack on the substrate urea [15]. This proposal was suggested by the observation of the position of $Asp^{\alpha363}$ Oδ2, placed between the Ni-bridging DAP oxygen (at 2.5 Å) and the "distal" DAP oxygen (at 3.5 Å). This proposal was further supported by the established conformational flexibility of the Cβ-Cα bond of $Asp^{\alpha363}$ in the structure of the BPU-AHA complex [19]. The structure of PHO-inhibited BPU seems to further strengthen this view, revealing the $Asp^{\alpha363}$ Oδ2 atom symmetrically interacting with the phosphate bridging oxygen (at 2.8 Å) and distal oxygen (at 3.0 Å). However, it appears that $Asp^{\alpha363}$ Oδ2 is protonated both in the DAP-BPU and PHO-BPU complexes, even though the presence or absence of this proton cannot be definitely proven at this resolution. This conclusion would present a major argument against $Asp^{\alpha363}$ Oδ2 acting as a proton donor, possibly suggesting that it remains protonated after the formation of the tetrahedral transition state formed upon the bridging hydroxide nucleophilic attack on the urea C atom. However, the structure of the PHO-BPU complex allows the assignment of the $pK_a = 6.3$–6.5 to the deprotonation of $Asp^{\alpha363}$ Oδ2 (as discussed above), this process being catalytically significant [5, 7], further supporting the proposed role of this residue as proton donor during catalysis.

In their latest report, Hausinger and colleagues [39] criticized our proposed role of proton donor for $Asp^{\alpha363}$ Oδ2 on the basis that the proton transfer from the bridging hydroxide to the distal NH_2 group of urea was considered "very unlikely". A further argument against it was stated to be the difficulty of removing the H-atom from the bridging hydroxide, supposed to have a high pK_a. This second point can be disputed by considering that the proton would be released from an intermediate containing an OH moiety bridging the divalent Ni ions through the oxygen atom and bound to an sp^3 carbon. Such a moiety, essentially an alcohol, is expected indeed to be very acidic and prone to release the proton. One example of such a decrease of the pK_a of metal-bound alcohols is provided by alcohol dehydrogenase, where the substrate alcohol experiences a large shift of pK_a (from 16 to 6.4) upon binding to the active site Zn(II) ion [42].

A water molecule as proton donor

This is a novel possibility that we wish to propose here. Owing to the increase of its pK_a upon or after hydroxide nucleophilic attack on the substrate, the nascent distal urea NH_2 sp^3 lone pair would easily accept a proton from a water molecule, and the new C-NH_3^+ group would be stabilized by H-bonding to the $His^{\alpha323}$ Nϵ in the closed flap conformation. Indeed, in the structure of the PHO-BPU complex there is a water molecule held between the distal phosphate O and $Arg^{\alpha339}$ through H-bonds (see Figs. 4 and 5), in the same position where we find sulfate in the structure of the native form and $His^{\alpha323}$ in the DAP-inhibited form of BPU [15]. This could be the very water molecule that donates a proton to the distal N of the intermediate formed after nucleophilic attack of the bridging hydroxide to the urea molecule. The role of $Arg^{\alpha339}$ would be to decrease the pK_a of that water molecule. Again, the structure of the PHO-BPU complex is critical in revealing the presence of such a water molecule positioned in a catalytically relevant position. A similarly positioned water molecule was observed both in the BPU-BME [18] and BPU-AHA [19] complexes, indicating that the active site structure favors the presence of a solvent molecule in this critical position.

The proton transfer from this "donor" water could be achieved by finely tuned machinery. When the flap moves from the open to the closed conformation, $His^{\alpha323}$ Nδ could establish a strong hydrogen bond with $Asp^{\alpha224}$ Oδ2 (2.9 Å in DAP-BPU). This interaction would influence the orientation and raise the pK_a of $His^{\alpha323}$ so it could accept a proton on its Nϵ (or better stabilize the C-NH_3^+ moiety). The proton donor water can then move from its original position, being replaced by $His^{\alpha323}$ (itself now possibly in its protonated form). When the flap moves to the completely closed conformation, $Arg^{\alpha339}$ moves by about 1 Å (as in the DAP-BPU structure) to a position such as to establish an unusual interaction with $His^{\alpha323}$ Nϵ, with one of its NH_2 protons pointing to the p-orbital of $His^{\alpha323}$ Nϵ located at a distance of 2.9 Å (DAP-BPU). This interaction would reduce the pK_a of $His^{\alpha323}$, favoring the transfer of the proton from $His^{\alpha323}$ Nϵ to the

distal urea NH_2 (or increase the "ammonia" character of the distal N atom of the intermediate).

In addition to the above discussion, it must be stated that the nucleophilic attack, the protonation of the distal N, and the breakage of the C-N bond could occur through a concerted process, thereby avoiding having two transition states. The order of events is not possible to resolve from the crystallographic structures of the ground, or native, state of the enzyme and the two tetrahedral transition state analogues DAP and PHO.

Conclusions

Much progress has been made in recent years towards a full understanding of the catalytic hydrolysis of urea, a fundamental process for both basic biochemistry as well as applied environmental, agricultural, and medical sciences, through the use of high-resolution protein crystallography. The formation of the tetrahedral transition state firmly reconciles all the experimental data. However, at present it is not possible to make an absolute choice among all the alternative pathways for the donation of a proton to the nascent ammonium group using the crystallographic evidence alone or, we believe, from any other evidence currently available. The results presented in this study, as well as the detailed discussion of their possible implications, should be profitable for a wider and deeper understanding of the catalytic mechanism of this important enzyme, as well as provide more general ideas about the functioning of binuclear metallic hydrolases. These hypotheses should be useful for the development of drugs able to diminish the negative effects of urease in human and animal health [11, 43, 44], as well as in the agricultural environment [43, 45, 46].

Acknowledgements We thank the European Union for support of the work at EMBL Hamburg through the HCMP Access to Large Installations Project, Contract Number CHGE-CT93-0040. S.C. and S.M. acknowledge funding by MURST, Progetti di Interesse Nazionale (ex-40% 1997 and 1999). S.B. thanks EMBL for a predoctoral fellowship. The authors are indebted to Dr. Silvia Miletti for preparing the enzyme samples. The YSBL is supported by a grant, number 87/SB09829, from the BBSRC as a Structural Biology Center.

References

1. Howell SP, Sumner JB (1934) J Biol Chem 104:619–626
2. Harmon KM, Niemann C (1949) J Biol Chem 177:601–605
3. Kistiakowsky GB, Mangelsdorf PS, Rosenberg AJ, Shaw WHR (1952) J Am Chem Soc 74:5015–5020
4. Dixon NE, Blakeley RL, Zerner B (1980) Can J Biochem 58:481–488
5. Todd MJ, Hausinger RP (1989) J Biol Chem 264:15835–15842
6. Huang TC, Chen DH (1991) J Chem Technol Biotechnol 52:433–444
7. Krajewska B, Zaborska W (1999) J Mol Catal B 6:75–81
8. Takishima K, Suga T, Mamiya G (1988) Eur J Biochem 175:151–165
9. Riddles PW, Whan V, Blakeley RL, Zerner B (1991) Gene 108:265–267
10. Mulrooney SB, Hausinger RP (1990) J Bacteriol 172:5837–5843
11. Mobley HLT, Island MD, Hausinger RP (1995) Microbiol Rev 59:451–480
12. Park I-S, Hausinger RP (1993) J Protein Chem 12:51–56
13. Park I-S, Hausinger RP (1993) Protein Sci 2:1034–1041
14. Jabri E, Carr MB, Hausinger RP, Karplus PA (1995) Science 268:998–1004
15. Benini S, Rypniewski WR, Wilson KS, Miletti S, Ciurli S, Mangani S (1999) Struct Fold Des 7:205–216
16. Ciurli S, Benini S, Rypniewski WR, Wilson KS, Miletti S, Mangani S (1999) Coord Chem Rev 190–192:331–355
17. Benini S, Ciurli S, Nolting HF, Mangani S (1996) Eur J Biochem 239:61–66
18. Benini S, Rypniewski WR, Wilson KS, Ciurli S, Mangani S (1998) JBIC 3:268–273
19. Benini S, Rypniewski WR, Wilson KS, Miletti S, Ciurli S, Mangani S (2000) JBIC 5:110–118
20. Andrews RK, Dexter A, Blakeley RL, Zerner B (1986) J Am Chem Soc 108:7124–7125
21. Musiani F, Arnofi E, Casadio R, Ciurli S (2001) JBIC 3:300–314
22. Benini S, Gessa C, Ciurli S (1996) Soil Biol Biochem 28:819–821
23. Otwinowski Z, Minor W (1997) Methods Enzymol 276:307–325
24. Dauter Z (1997) Methods Enzymol 276:326–344
25. Jones TA, Zou JY, Cowan SW, Kjeldgaard M (1991) Acta Crystallogr Sect A 47:110–119
26. Murshudov GN, Vagin AA, Dodson EJ (1997) Acta Crystallogr Sect D 53:240–255
27. Engh RA, Huber R (1991) Acta Crystallogr Sect A 47:392–400
28. Lamzin VS, Wilson KS (1997) Methods Enzymol 277:269–305
29. Vriend G (1990) J Mol Graph 8:52–56
30. Laskowski RA, MacArthur MW, Moss DS, Thornton JM (1993) J Appl Crystallogr 26:283–291
31. Karplus PA, Pearson MA, Hausinger RP (1997) Acc Chem Res 30:330–337
32. Benini S (2000) PhD thesis, University of York, UK
33. Kimura E (2000) Curr Opin Chem Biol 4:207–213
34. Bashkin JK (1999) Curr Opin Chem Biol 3:752–758
35. Addison AW, Rao TN, Reedijk J, van Rijn J, Verschoor GC (1984) J Chem Soc Dalton Trans 1349–1356
36. Luecke H, Quiocho FA (1990) Nature 347:402–406
37. Pflugrath JW, Quiocho FA (1985) Nature 314:257–260
38. Todd MJ, Hausinger RP (2000) Biochemistry 39:5389–5396
39. Pearson MA, Park IS, Schaller RA, Michel LO, Karplus PA, Hausinger RP (2000) Biochemistry 39:8575–8584
40. Barrios AM, Lippard SJ (1999) J Am Chem Soc 121:11751–11757
41. Sinnott ML (ed) (1998) Comprehensive biological catalysis. Academic Press, San Diego
42. Kvassman J, Pettersson G (1980) Eur J Biochem 103:557–564
43. Mobley HLT, Hausinger RP (1989) Microbiol Rev 53:85–108
44. Collins CM, D'Orazio SEF (1993) Mol Microbiol 9:907–913
45. Bremner JM, Krogmeier MJ (1989) Proc Natl Acad Sci USA 86:8185–8188
46. Bremner JM (1995) Fert Res 42:321–329